Measurements with photonic events in e^+e^- collisions at centre-of-mass energies of 130-140 GeV

OPAL Collaboration

G. Alexander[w], J. Allison[p], N. Altekamp[e], K. Ametewee[y], K.J. Anderson[i], S. Anderson[ℓ],
S. Arcelli[b], S. Asai[x], D. Axen[ac], G. Azuelos[r,1], A.H. Ball[q], E. Barberio[z], R.J. Barlow[p],
R. Bartoldus[c], J.R. Batley[e], G. Beaudoin[r], J. Bechtluft[n], C. Beeston[p], T. Behnke[h],
A.N. Bell[a], K.W. Bell[t], G. Bella[w], S. Bentvelsen[h], P. Berlich[j], S. Bethke[n], O. Biebel[n],
V. Blobel[h], I.J. Bloodworth[a], J.E. Bloomer[a], P. Bock[k], H.M. Bosch[k], M. Boutemeur[r],
B.T. Bouwens[ℓ], S. Braibant[ℓ], R.M. Brown[t], H.J. Burckhart[h], C. Burgard[aa], R. Bürgin[j],
P. Capiluppi[b], R.K. Carnegie[f], A.A. Carter[m], J.R. Carter[e], C.Y. Chang[q], C. Charlesworth[f],
D.G. Charlton[a,2], D. Chrisman[d], S.L. Chu[d], P.E.L. Clarke[o], I. Cohen[w], J.E. Conboy[o],
O.C. Cooke[p], M. Cuffiani[b], S. Dado[v], C. Dallapiccola[q], G.M. Dallavalle[b], C. Darling[ae],
S. De Jong[ℓ], L.A. del Pozo[h], M.S. Dixit[g], E. do Couto e Silva[ℓ], M. Doucet[r],
E. Duchovni[z], G. Duckeck[h], I.P. Duerdoth[p], J.E.G. Edwards[p], P.G. Estabrooks[f],
H.G. Evans[i], M. Evans[m], F. Fabbri[b], P. Fath[k], F. Fiedler[ℓ], M. Fierro[b], H.M. Fischer[c],
R. Folman[z], D.G. Fong[q], M. Foucher[q], H. Fukui[x], A. Fürtjes[h], P. Gagnon[g], A. Gaidot[u],
J.W. Gary[d], J. Gascon[r], S.M. Gascon-Shotkin[q], N.I. Geddes[t], C. Geich-Gimbel[c],
S.W. Gensler[i], F.X. Gentit[u], T. Geralis[t], G. Giacomelli[b], P. Giacomelli[d], R. Giacomelli[b],
V. Gibson[e], W.R. Gibson[m], D.M. Gingrich[ad,1], J. Goldberg[v], M.J. Goodrick[e], W. Gorn[d],
C. Grandi[b], E. Gross[z], M. Gruwé[h], C. Hajdu[af], G.G. Hanson[ℓ], M. Hansroul[h], M. Hapke[m],
C.K. Hargrove[g], P.A. Hart[i], C. Hartmann[c], M. Hauschild[h], C.M. Hawkes[e], R. Hawkings[h],
R.J. Hemingway[f], G. Herten[j], R.D. Heuer[h], M.D. Hildreth[h], J.C. Hill[e], S.J. Hillier[a],
T. Hilse[j], P.R. Hobson[y], R.J. Homer[a], A.K. Honma[ab,1], D. Horváth[af,3], R. Howard[ac],
R.E. Hughes-Jones[p], D.E. Hutchcroft[e], P. Igo-Kemenes[k], D.C. Imrie[y], M.R. Ingram[p],
A. Jawahery[q], P.W. Jeffreys[t], H. Jeremie[r], M. Jimack[a], A. Joly[r], G. Jones[p], M. Jones[f],
R.W.L. Jones[h], U. Jost[k], P. Jovanovic[a], J. Kanzaki[x], D. Karlen[f], T. Kawamoto[x],
R.K. Keeler[ab], R.G. Kellogg[q], B.W. Kennedy[t], J. King[m], J. Kirk[ac], S. Kluth[h],
T. Kobayashi[x], M. Kobel[j], D.S. Koetke[f], T.P. Kokott[c], S. Komamiya[x], R. Kowalewski[h],
T. Kress[k], P. Krieger[f], J. von Krogh[k], P. Kyberd[m], G.D. Lafferty[p], H. Lafoux[u],
R. Lahmann[q], W.P. Lai[s], D. Lanske[n], J. Lauber[o], J.G. Layter[d], A.M. Lee[ae], E. Lefebvre[r],
D. Lellouch[z], J. Letts[b], L. Levinson[z], C. Lewis[o], S.L. Lloyd[m], F.K. Loebinger[p],

G.D. Long[q], B. Lorazo[r], M.J. Losty[g], J. Ludwig[j], A. Luig[j], A. Malik[u], M. Mannelli[h],
S. Marcellini[h], C. Markus[c], A.J. Martin[m], J.P. Martin[r], G. Martinez[q], T. Mashimo[x],
W. Matthews[y], P. Mättig[c], W.J. McDonald[ad], J. McKenna[ac], E.A. Mckigney[o],
T.J. McMahon[a], A.I. McNab[m], F. Meijers[h], S. Menke[c], F.S. Merritt[i], H. Mes[g],
J. Meyer[aa], A. Michelini[h], G. Mikenberg[z], D.J. Miller[o], R. Mir[z], W. Mohr[j],
A. Montanari[b], T. Mori[x], M. Morii[x], U. Müller[c], B. Nellen[c], B. Nijjhar[p], R. Nisius[h],
S.W. O'Neale[a], F.G. Oakham[g], F. Odorici[b], H.O. Ogren[ℓ], T. Omori[x], M.J. Oreglia[i],
S. Orito[x], M. Palazzo[b], J. Pálinkás[ag,4], J.P. Pansart[u], G. Pásztor[af], J.R. Pater[p],
G.N. Patrick[t], M.J. Pearce[a], S. Petzold[aa], J.E. Pilcher[i], J. Pinfold[ad], D.E. Plane[h],
P. Poffenberger[ab], B. Poli[b], A. Posthaus[c], H. Przysieznïak[ad], D.L. Rees[a], D. Rigby[a],
M.G. Rison[e], S.A. Robins[m], N. Rodning[ad], J.M. Roney[ab], A. Rooke[o], E. Ros[h],
A.M. Rossi[b], M. Rosvick[ab], P. Routenburg[ad], Y. Rozen[h], K. Runge[j], O. Runolfsson[h],
D.R. Rust[ℓ], R. Rylko[y], E.K.G. Sarkisyan[w], M. Sasaki[x], C. Sbarra[b], A.D. Schaile[h,5],
O. Schaile[j], F. Scharf[c], P. Scharff-Hansen[h], P. Schenk[d], B. Schmitt[c], M. Schröder[h],
H.C. Schultz-Coulon[j], M. Schulz[h], P. Schütz[c], J. Schwiening[c], W.G. Scott[t], T.G. Shears[p],
B.C. Shen[d], C.H. Shepherd-Themistocleous[aa], P. Sherwood[o], G.P. Siroli[b], A. Sittler[aa],
A. Skillman[o], A. Skuja[q], A.M. Smith[h], T.J. Smith[ab], G.A. Snow[q], R. Sobie[ab],
S. Söldner-Rembold[j], R.W. Springer[ad], M. Sproston[t], A. Stahl[c], M. Starks[ℓ], K. Stephens[p],
J. Steuerer[aa], B. Stockhausen[c], D. Strom[s], F. Strumia[h], P. Szymanski[t], R. Tafirout[r],
H. Takeda[x], P. Taras[r], S. Tarem[v], M. Tecchio[h], N. Tesch[c], M. Thiergen[j], M.A. Thomson[h],
E. von Törne[c], S. Towers[f], M. Tscheulin[j], E. Tsur[w], A.S. Turcot[i], M.F. Turner-Watson[h],
P. Utzat[k], R. Van Kooten[ℓ], G. Vasseur[u], M. Verzocchi[j], P. Vikas[r], M. Vincter[ab],
E.H. Vokurka[p], F. Wäckerle[j], A. Wagner[aa], C.P. Ward[e], D.R. Ward[e], J.J. Ward[o],
P.M. Watkins[a], A.T. Watson[a], N.K. Watson[g], P. Weber[f], P.S. Wells[h], N. Wermes[c],
J.S. White[ab], B. Wilkens[j], G.W. Wilson[aa], J.A. Wilson[a], T. Wlodek[z], G. Wolf[z],
S. Wotton[k], T.R. Wyatt[p], S. Xella[b], S. Yamashita[x], G. Yekutieli[z], K. Yoshimura[x],
V. Zacek[r]

[a] *School of Physics and Space Research, University of Birmingham, Birmingham B15 2TT, UK*
[b] *Dipartimento di Fisica dell' Università di Bologna and INFN, I-40126 Bologna, Italy*
[c] *Physikalisches Institut, Universität Bonn, D-53115 Bonn, Germany*
[d] *Department of Physics, University of California, Riverside CA 92521, USA*
[e] *Cavendish Laboratory, Cambridge CB3 0HE, UK*
[f] *Ottawa-Carleton Institute for Physics, Department of Physics, Carleton University, Ottawa, Ontario K1S 5B6, Canada*
[g] *Centre for Research in Particle Physics, Carleton University, Ottawa, Ontario K1S 5B6, Canada*
[h] *CERN, European Organisation for Particle Physics, CH-1211 Geneva 23, Switzerland*
[i] *Enrico Fermi Institute and Department of Physics, University of Chicago, Chicago IL 60637, USA*
[j] *Fakultät für Physik, Albert Ludwigs Universität, D-79104 Freiburg, Germany*
[k] *Physikalisches Institut, Universität Heidelberg, D-69120 Heidelberg, Germany*
[ℓ] *Indiana University, Department of Physics, Swain Hall West 117, Bloomington IN 47405, USA*
[m] *Queen Mary and Westfield College, University of London, London E1 4NS, UK*
[n] *Technische Hochschule Aachen, III Physikalisches Institut, Sommerfeldstrasse 26-28, D-52056 Aachen, Germany*
[o] *University College London, London WC1E 6BT, UK*
[p] *Department of Physics, Schuster Laboratory, The University, Manchester M13 9PL, UK*
[q] *Department of Physics, University of Maryland, College Park, MD 20742, USA*
[r] *Laboratoire de Physique Nucléaire, Université de Montréal, Montréal, Quebec H3C 3J7, Canada*

ˢ *University of Oregon, Department of Physics, Eugene OR 97403, USA*

ᵗ *Rutherford Appleton Laboratory, Chilton, Didcot, Oxfordshire OX11 0QX, UK*

ᵘ *CEA, DAPNIA/SPP, CE-Saclay, F-91191 Gif-sur-Yvette, France*

ᵛ *Department of Physics, Technion-Israel Institute of Technology, Haifa 32000, Israel*

ʷ *Department of Physics and Astronomy, Tel Aviv University, Tel Aviv 69978, Israel*

ˣ *International Centre for Elementary Particle Physics and Department of Physics, University of Tokyo, Tokyo 113, Japan
and Kobe University, Kobe 657, Japan*

ʸ *Brunel University, Uxbridge, Middlesex UB8 3PH, UK*

ᶻ *Particle Physics Department, Weizmann Institute of Science, Rehovot 76100, Israel*

ᵃᵃ *Universität Hamburg/DESY, II Institut für Experimental Physik, Notkestrasse 85, D-22607 Hamburg, Germany*

ᵃᵇ *University of Victoria, Department of Physics, P O Box 3055, Victoria BC V8W 3P6, Canada*

ᵃᶜ *University of British Columbia, Department of Physics, Vancouver BC V6T 1Z1, Canada*

ᵃᵈ *University of Alberta, Department of Physics, Edmonton AB T6G 2J1, Canada*

ᵃᵉ *Duke University, Department of Physics, Durham, NC 27708-0305, USA*

ᵃᶠ *Research Institute for Particle and Nuclear Physics, H-1525 Budapest, PO Box 49, Hungary*

ᵃᵍ *Institute of Nuclear Research, H-4001 Debrecen, PO Box 51, Hungary*

Abstract

Cross-sections and angular distributions for the production of events with single and multiple photons are measured from data recorded with the OPAL detector at the recently upgraded LEP collider. The measured cross-sections are generally consistent with Standard Model expectations for the $e^+e^- \rightarrow \nu\bar{\nu}\gamma(\gamma)$ and $e^+e^- \rightarrow \gamma\gamma(\gamma)$ processes. Six events with an acoplanar photon pair and large missing mass are found. The observed number of events is larger than expected from $e^+e^- \rightarrow \nu\bar{\nu}\gamma\gamma$; however, the missing mass distribution is compatible with the Z^0 resonance. Deviations from QED are constrained by the data on $e^+e^- \rightarrow \gamma\gamma(\gamma)$. Lower limits are set at 95% confidence level on the QED cut-off parameters Λ_+ and Λ_- of 152 GeV and 142 GeV, respectively, and also on the mass of an excited electron of 147 GeV.

1. Introduction

Measurements of cross-sections and angular distributions are presented for events produced in e^+e^- collisions with one and more photons and no other observed particles. These data with centre-of-mass energies, $\sqrt{s}$, in the range 130 to 140 GeV were recorded by the OPAL experiment at LEP in October and November 1995. These are the highest energy e^+e^- collision data yet available and the first at energies well above the Z^0 resonance. The motivation is therefore to extend measurements to this new energy domain and to search for new particles beyond the

mass limits established from e^+e^- collisions at lower centre-of-mass energies.

Event topologies

Three, not mutually exclusive, experimental topologies for events with photon(s) and zero charged multiplicity have been studied. The topologies are defined largely following the experimental techniques and, in part, the physics motivations of previous publications by the OPAL Collaboration based on data obtained at the Z^0 resonance [1-3]. The acceptance of each topology is defined in terms of the photon energy, E_γ, scaled to the beam energy, ($x_\gamma \equiv E_\gamma/E_{\text{beam}}$), and the polar angle of the photon, θ, defined with respect to the electron beam direction. The first two topologies are designed to select events with significant transverse momentum imbalance thus signalling the presence of at least one neutrino-like invisible particle which inter-

---

¹ and at TRIUMF, Vancouver, Canada V6T 2A3.

² and Royal Society University Research Fellow.

³ and Institute of Nuclear Research, Debrecen, Hungary.

⁴ and Department of Experimental Physics, Lajos Kossut Debrecen, Hungary.

⁵ and Ludwig-Maximilians-Universität, München, Germany.

acts only weakly with matter. Besides the known neutrino species, hypothesised particles such as the scalar neutrino or the lightest neutralino ($\tilde{\chi}_1^0$) of supersymmetry theories can also be considered as invisible particles. The third topology is events with at least two energetic photons and is expected to be dominated by the purely QED process $e^+e^- \to \gamma\gamma(\gamma)$. The definition of each topology is listed below:

Topology A: One or two photons accompanied by invisible particle(s) ($e^+e^- \to \gamma(\gamma)+$ invisible particle(s)). At least one photon with $x_\gamma > 0.2$ and $|\cos\theta| < 0.7$.

Topology B: Acoplanar photon pair ($e^+e^- \to \gamma\gamma+$ invisible particle(s)). Two photons each with energy exceeding 1.75 GeV and $|\cos\theta| < 0.7$.

Topology C: Two or more photons ($e^+e^- \to \gamma\gamma + \geq 0$ neutral particles). At least two photons with $x_\gamma > 0.2$ and $15° < \theta < 165°$. Additional photons but also possible invisible particles are considered as neutral particles.

Topology A is sensitive to the production of one or two photons and missing energy, which within the Standard Model is expected to arise from the $e^+e^- \to \nu\bar{\nu}\gamma(\gamma)$ process. Measurements of single photon production have been made in e^+e^- collisions on the Z^0 and at lower energies [4,1,5]. Of special interest has been the direct measurement of the Z^0 invisible width. The centre-of-mass energies attained now at LEP allow the observation for the first time of the striking experimental signature of a highly energetic photon recoiling against a real Z^0 decaying invisibly, as envisaged in the original "neutrino counting" proposals [6]. The expected visible energies are sufficiently large at the present centre-of-mass energies that doubly radiative neutrino production can lead to two photons being detected and therefore the experimental topology has been extended to include such cases. The single photon topology is also a rich hunting ground for many types of new physics in e^+e^- collisions (see e.g. [1,7] and references therein). Examples of possible new physics, particularly of interest at these energies, are $e^+e^- \to \gamma X$ with X a new invisible particle or possessing invisible decay modes and the production of invisible particles made visible simply through initial state radiation. Given the now well established three generations of light neutrinos, the present measurement is relevant to possible heavy invisible particles (generally with mass greater

than about $m_Z/2$) produced in association with initial state radiation. A further example is $e^+e^- \to \tilde{\chi}_1^0\tilde{\chi}_2^0$ with the second lightest neutralino, $\tilde{\chi}_2^0$, decaying radiatively to the lightest neutralino, $\tilde{\chi}_2^0 \to \tilde{\chi}_1^0\gamma$. The branching ratio for the radiative decay is usually small but can be dominant in some regions of supersymmetry parameter space [8]. The single photon topology has also been discussed [9] as a method to tag using initial state radiation "almost invisible particles" such as charginos or the $\tilde{\chi}_2^0$ when they are almost mass-degenerate with their invisible decay product, usually the lightest neutralino, $\tilde{\chi}_1^0$.

Search topology B is sensitive to the possible pair production of neutral particles X, followed by radiative decay to an invisible particle Y. Such a process, $e^+e^- \to XX \to YY\gamma\gamma$, could occur for pair production of $\tilde{\chi}_2^0$ followed by the radiative decay discussed above or excited neutrino pair production. It is also of interest in the context of the production in association with invisible particle(s) of a new particle X with a decay mode to two photons as discussed in [2].

The inclusive measurement of neutral events with at least two energetic photons (topology C) is motivated both as a test at these high energies of the expected purely QED process $e^+e^- \to \gamma\gamma(\gamma)$ and as a measurement sensitive to neutral events with higher photon multiplicities. The higher centre-of-mass energies allow one to extend the energy scale over which QED has been tested and allow one to constrain possible new particles such as excited electrons. Similar investigations have been carried out previously at low energy and at the Z^0 [3,10,11]. The experimental topology as defined is also sensitive to processes with missing energy such as those discussed for topology B if the photons satisfy the acceptance. For a hypothesised new particle X with a decay mode to two photons, topology C is sensitive to the production of X in two-photon collisions followed by decay to two photons, and the production of X in association with a photon leading to a three-photon final state [2].

All three topologies are sensitive to doubly radiative neutrino production, $e^+e^- \to \nu\bar{\nu}\gamma\gamma$. This process, with an observable cross-section at these centre-of-mass energies, is considered as part of the radiative correction of the inclusive single photon measurement in topology A, while for topology B, it represents the essentially irreducible Standard Model background to a search for new physics processes. Topology C is ex-

pected to be dominated by the $e^+e^- \rightarrow \gamma\gamma(\gamma)$ process with a small but separable contribution from $e^+e^- \rightarrow \nu\bar{\nu}\gamma\gamma$.

In the following, we first describe the data-sample and general methods used. Then, for each topology, the event selection is described and the results are presented.

2. Data-sample and methods

The OPAL detector is described in detail elsewhere [12]. The measurements presented here are mainly based on the observation of clusters of energy deposited in the lead-glass electromagnetic calorimeters. These calorimeters together with the gamma-catcher calorimeter and forward detector provide a fully hermetic electromagnetic calorimeter down to polar angles of 60 mrad. The tracking system, consisting of a silicon micro-vertex detector, a vertex drift chamber and a large volume jet drift chamber, is used to select events consistent with zero charged multiplicity. Backgrounds from cosmic-ray interactions are controlled using time-of-flight information and the hadron calorimeter and muon detectors.

The data used in this analysis were recorded at e^+e^- centre-of-mass energies of 130.26, 136.23 and 140.2 GeV, with integrated luminosities of 2.64, 2.54 and 0.038 pb^{-1}, respectively. The centre-of-mass energy of the collisions at the OPAL interaction point is known with an uncertainty of 60 MeV [13]. The integrated luminosity was measured with a precision of 1% using small-angle Bhabha scattering in the forward calorimetry as described in [14].

Monte Carlo simulation studies were performed for signal and background processes. For $e^+e^- \rightarrow \nu\bar{\nu}\gamma(\gamma)$ and $e^+e^- \rightarrow \gamma\gamma(\gamma)$ we used the NNGG03 [15] and the RADCOR [16] programs respectively. For $e^+e^- \rightarrow e^+e^-$ we used the BABAMC and TEEGG [17] programs and for $e^+e^- \rightarrow \mu^+\mu^-$ and $e^+e^- \rightarrow \tau^+\tau^-$ the KORALZ program [18]. All samples were processed through the OPAL detector simulation [19].

3. Topology A: Events with one or two photons and invisible particle(s)

Single photon events are selected based on a subset of the criteria described in [1]. The selection requires that there is an electromagnetic cluster in the region $|\cos\theta| < 0.7$ identified by timing information as consistent with originating from the interaction point. Events with reconstructed tracks in the jet chamber and significant activity in the electromagnetic calorimeters, hadron calorimeter or muon chambers are rejected. We concentrate on high energy photons ($x_\gamma > 0.2$). Therefore some criteria designed for low energy photons have been loosened or removed in order to increase the efficiency and to simplify the analysis. In order to increase the efficiency for doubly radiative neutrino production, and so lessen the sensitivity to the modelling of this process, we also select events which fail only the second cluster veto (criterion C1 in Ref. [1]). That is, we include events which contain an additional electromagnetic cluster in the barrel or endcap calorimeter with deposited energy exceeding 300 MeV. The additional background from $e^+e^- \rightarrow \gamma\gamma(\gamma)$ is rejected if any of the following criteria are satisfied:

- A third electromagnetic cluster is detected with deposited energy exceeding 300 MeV.
- The missing momentum vector calculated from the two clusters satisfies $|\cos\theta_{\mathrm{miss}}| > 0.9$.
- The acoplanarity angle of the two clusters [6], ϕ_{acop}, is less than 2.5°.
- The total energy of the two clusters exceeds 90% of the centre-of-mass energy.

In total 19 events are selected.

Cross-sections are measured for the kinematic acceptance $x_\gamma > 0.2$ and $|\cos\theta| < 0.7$ and the efficiency is evaluated within this acceptance using the Monte Carlo event generator described in [15]. This includes doubly radiative neutrino production but only for the dominant Z^0 diagrams. The efficiency for detecting $\nu\bar{\nu}\gamma(\gamma)$ is estimated to be $(70 \pm 2)\%$ at each centre-of-mass energy. Here and throughout the paper, the quoted errors on efficiencies include estimates of systematic errors which are small compared to the statistical errors on the measurements. Background

---

[6] Defined as 180° minus the opening angle in the transverse plane.

Table 1

Numbers of events selected (N_{sel}) and measured cross-sections. All quoted cross-sections are for the kinematic acceptance stated and have been corrected for the detection efficiency within that acceptance. For the cross-sections, the error shown is statistical only. Systematic errors on the cross-sections are small but common to each energy point, amounting to 3% for the $\gamma(\gamma)$ +invisible(s) topology, 5% for $\gamma\gamma$+invisible(s) and 2% for the $\gamma\gamma+ \geq 0$ neutrals topology. Also shown are the Standard Model predictions (σ^{SM}) using the Monte Carlo calculations of [16] and [20] for $\gamma\gamma(\gamma)$ and $\nu\bar{\nu}\gamma(\gamma)$ production, respectively. The expectation for $\gamma\gamma$+invisible(s) was evaluated using the Monte Carlo calculation of Ref. [15]. The rows labelled $\gamma\gamma(\gamma)$ are calculated after applying the recoil mass cut at 70 GeV to reject the expected contribution from $\nu\bar{\nu}\gamma\gamma$.

Channel	$\sqrt{s}$ (GeV)	N_{sel}	σ (pb)	σ^{SM} (pb)
$\gamma(\gamma)$+invisible(s) ($x_\gamma > 0.2$; $\|\cos\theta\| < 0.7$)	130.26	6	3.3±1.3	5.0
	136.23	13	7.2±2.0	4.2
	140.2	0	—	3.8
$\gamma\gamma$+invisible(s) ($E_\gamma > 1.75$ GeV; $\|\cos\theta\| < 0.7$)	133	4	1.1±0.5	0.19
$\gamma\gamma+ \geq 0$ neutrals ($x_\gamma > 0.2$; $15° < \theta < 165°$)	130.26	59	24.6±3.2	25.2
	136.23	42	18.2±2.8	23.0
	140.2	1	29±29	21.7
$\gamma\gamma(\gamma)$ ($x_\gamma > 0.2$; $15° < \theta < 165°$)	130.26	58	24.1±3.2	25.0
	136.23	42	18.2±2.8	22.8
	140.2	1	29±29	21.5

contributions have been considered, notably $e^+e^- \rightarrow \gamma\gamma(\gamma)$, and are estimated to be negligible. The number of events selected and the inclusive cross-sections are reported in Table 1. The $\cos\theta$ distribution of the most energetic photon is shown in Fig. 1(a), while the measured distribution of the mass recoiling against the photon(s), i.e. the missing mass, M_{miss}, is shown in Fig. 1(c). One observes that the angular distribution is consistent with expectation and that most events are consistent with real Z^0 production as expected. Fig. 2 shows the measured cross-section compared to the expectation evaluated using the Monte Carlo event generator recently developed for LEP2 energies [20] using the structure function formalism.

We also wish to investigate non-Z^0 effects such as t-channel W exchange and new physics scenarios like those discussed in the introduction while reducing the sensitivity to the dominant radiative return to the Z^0. The measured cross-sections for $x_\gamma > 0.2$ and $M_{miss} > M_Z + 10$ GeV are (0.5 ± 0.5) pb and (1.7 ± 1.0) pb at 130.26 and 136.23 GeV, respectively, in agreement with expectation (see Fig. 2). No events are observed with $x_\gamma > 0.2$ and $M_{miss} < M_Z - 10$ GeV. Combining the centre-of-mass energies ($\langle\sqrt{s}\rangle = 133$ GeV), we obtain an upper limit at 95% confidence level (CL) of 0.9 pb on the latter cross-section.

Table 2

Kinematic characteristics of the six events with an acoplanar photon pair selected in the three topologies. The quantities listed are the centre-of-mass energy, the energies of each photon (ordered in energy), the acoplanarity angle of the two photons (in degrees), the missing mass and the mass of the two photons. The units are GeV unless stated.

Topology	$\sqrt{s}$	E_1	E_2	ϕ_{acop}	M_{miss}	$M_{\gamma\gamma}$
A	130.26	31.9	2.9	31.4	90.0 ± 1.9	13.6 ± 0.9
A,B	130.26	29.4	5.9	55.1	91.2 ± 1.7	23.3 ± 1.1
A,B	136.23	35.2	4.8	125.4	88.3 ± 2.2	11.9 ± 0.6
A,B	136.23	35.2	2.2	83.2	92.4 ± 2.0	13.1 ± 0.9
A,B	136.23	36.1	2.4	137.1	90.0 ± 2.2	6.8 ± 0.5
C	130.26	28.5	18.4	14.2	81.3 ± 1.7	42.9 ± 1.4

Five of the selected events have a detected second photon with deposited energy exceeding 300 MeV. Their kinematic characteristics are listed in Table 2. Fig. 1(b) shows the distribution, for events with two photons, of ϕ_{acop} versus M_{miss} prior to the cut on acoplanarity angle. The five selected events with two photons have a missing mass within 5 GeV of the Z^0 mass. The number of events expected with a detected second cluster from the modelled $\nu\bar{\nu}\gamma\gamma$ process is 2.1 ± 0.2. The observed number of events is thus higher than expected although the kinematic characteristics of these five events are consistent with $\nu\bar{\nu}\gamma\gamma$ mediated by the Z^0.

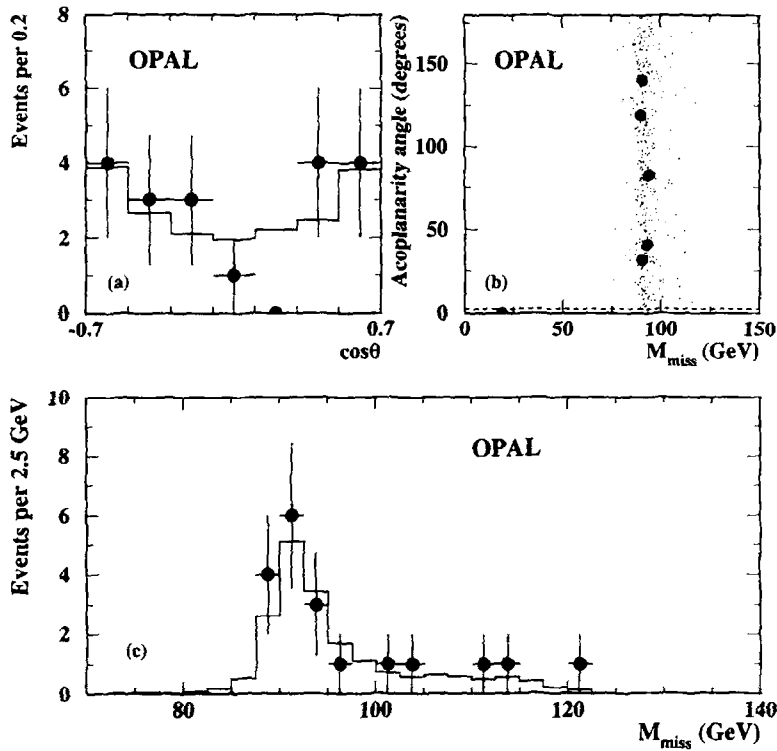OPAL Collaboration / Physics Letters B 377 (1996) 222–234

Fig. 1. Topology A. (a) Cosine of the polar angle of the most energetic photon. (b) Distribution of acoplanarity angle versus missing mass for events with at least two electromagnetic clusters with all selection criteria applied except the acoplanarity angle cut at 2.5°. The cut value is indicated by the dashed line; one event is removed by the cut. The events found in the data are displayed with large dots and the expected distribution for $\nu\bar{\nu}\gamma\gamma$ is shown using small dots for a sample size corresponding to the expectation for 200 times the integrated luminosity of the data. (c) The measured missing mass for the 19 selected events. In (a) and (c) the data are displayed as the points with error bars while the histograms indicate the expected distributions. For all histograms the expected distributions are evaluated with full detector simulation using [15].

4. Topology B: Events with an acoplanar photon pair

A specific search for neutral events with an acoplanar photon pair is presented. The acceptance overlaps partly with the measurements presented in topologies A and C but in this case the kinematic acceptance extends well below the $x_\gamma > 0.2$ requirements of the other analyses, thus allowing acceptance for events with very low visible energy.

The event selection for this topology broadly follows the search in the $\nu\bar{\nu}\gamma\gamma$ channel described in [2]. Events with reconstructed charged tracks are rejected. Candidate events are required to contain two photons each depositing at least 1.5 GeV in the electromagnetic calorimeter and detected in the region $|\cos\theta| < 0.7$. Following [1], the experimental requirement on

deposited energy exceeding 1.5 GeV corresponds to an effective minimum photon energy of 1.75 GeV. The restricted angular acceptance is chosen to discriminate against generally forward peaked backgrounds, to ensure a precise measurement of the photons and in order to verify using timing information that the photons are consistent with originating from the interaction point. Background from principally $e^+e^- \to \gamma\gamma(\gamma)$ is rejected if any of the four veto conditions described in topology A is satisfied.

Residual contamination from $e^+e^- \to \gamma\gamma(\gamma)$ is negligible. Background contributions from resonance production in two-photon collisions have been studied as described in [1] and can be neglected here. Defining the kinematical acceptance to be two photons with energy exceeding 1.75 GeV and $|\cos\theta| < 0.7$, the efficiency for $\nu\bar{\nu}\gamma\gamma$ detection is $(73 \pm 3)\%$.
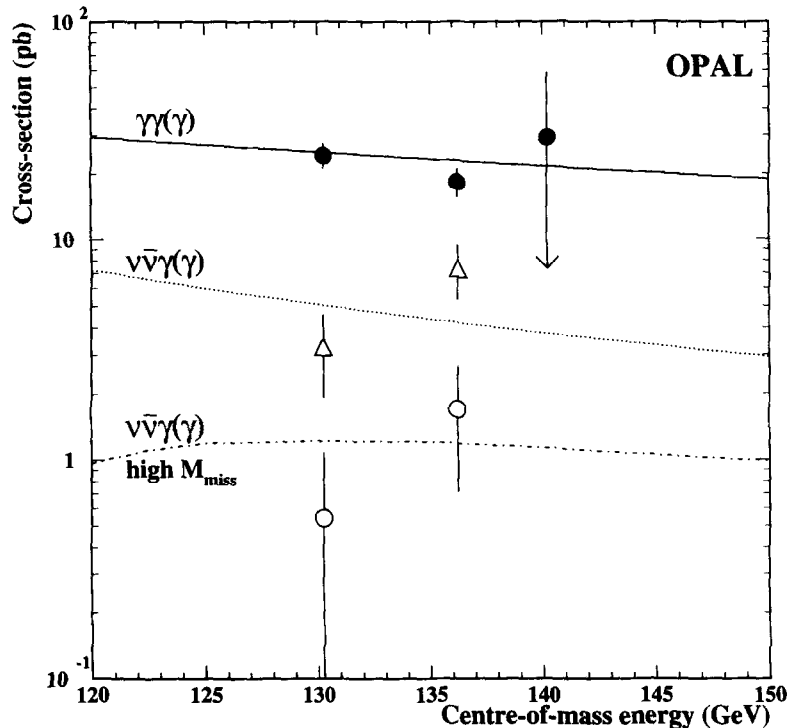
Fig. 2. The closed circles show the measured cross-sections for $e^+e^- \to \gamma\gamma(\gamma)$ compared with the expectation from $\mathcal{O}(\alpha^3)$ QED (solid line). The lower error bar on the 140 GeV point has been truncated for clarity. The remaining points and curves show the cross-sections for $\gamma(\gamma)+$ invisible particle(s). The open triangles represent the inclusive cross-section defined in terms of at least one photon with $x_\gamma > 0.2$ and $|\cos\theta| < 0.7$ at each centre-of-mass energy compared with the expectation evaluated with the Monte Carlo event generator described in [20] (dotted line). The measured cross-sections for events with $M_{miss} > M_Z + 10$ GeV are represented by the open circles, where the missing mass, M_{miss}, is defined as the recoil mass to the photon or two photons. The latter cross-sections are also compared with the above expectation (dot-dashed line).

Four events are selected from the data compared with 0.7 ± 0.1 events expected from the Standard Model process, $e^+e^- \to \nu\bar{\nu}\gamma\gamma$. No high mass candidates failing only the total energy cut are found. All four are common to the selection for topology A and none is common to topology C. The event characteristics are shown in Table 2. The di-photon mass of the events ranges from 7 to 23 GeV. Although more events are observed than expected, all four events have missing mass consistent with doubly radiative Z^0 production with subsequent decay of the Z^0 to neutrinos. The observed excess may be a statistical fluctuation of the expected $\nu\bar{\nu}\gamma\gamma$ events; the probability for observing at least four events when 0.7 events are expected is calculated to be 0.6%. The corresponding cross-section for $e^+e^- \to \gamma\gamma+$ invisible particle(s), evaluated using the $\nu\bar{\nu}\gamma\gamma$ production model and the kinematical accep-

tance defined above, is measured to be (1.1 ± 0.5) pb at an average centre-of-mass energy of 133 GeV compared to an expected cross-section of (0.19 ± 0.02) pb evaluated for $\nu\bar{\nu}\gamma\gamma$ with NNGG03 [15].

The efficiency for XX production and subsequent radiative decay of X to Y, where X could be $\tilde{\chi}_2^0$ and Y could be $\tilde{\chi}_1^0$, has been estimated assuming isotropic distributions for the production and decay angles. The efficiency to satisfy the kinematical acceptance and the acoplanarity angle requirement exceeds 45% for a wide range of masses for X and Y. Even for extreme cases such as $m_X = 2$ GeV and $m_Y = 0$ GeV, which lead to small acoplanarity angles, it exceeds 10%. Provided the photons have acoplanarity angles exceeding the cut, the experimental detection efficiency within the kinematical acceptance is greater than 80%. For the $\nu\bar{\nu}X$ search, where X decays to two photons, the

overall efficiency is estimated to be 40% for $m_X \approx$ 90 GeV based on the efficiency determined with the Z*X production model in [2]. Based on four events observed and an expected contribution of 0.7 events from known processes, we set an upper limit at 95% CL of 2.0 pb on the cross-section for the anomalous production of an acoplanar photon pair with acoplanarity angle exceeding 2.5° and where each photon has energy exceeding 1.75 GeV and $|\cos\theta| < 0.7$.

5. Topology C: Events with at least two photons

We present measurements of the cross-section and angular distribution for events with zero charged multiplicity and at least two hard photons. In order to retain a high efficiency down to polar angles of 15°, the event selection accepts events where the candidate photons are consistent with converting in the detector material as signalled by the presence of charged track activity at large radius, and the absence of track segments in the inner tracking detectors. The event selection proceeds in three steps.

Firstly, we select events with at least two electromagnetic clusters with x_γ exceeding 0.2 and polar angle in the range $15° < \theta < 165°$. In order to reduce kinematically backgrounds from Bhabha scattering in the (e)eγ topology (one electron unseen at low polar angle), we require that for events where the acoplanarity angle, ϕ_{acop}, of the two most energetic electromagnetic ("trigger") clusters is less than 5°:

$$x_z = \frac{2|\sin(\theta_1 + \theta_2)|}{|\sin(\theta_1 + \theta_2)| + \sin\theta_1 + \sin\theta_2} < 0.7,$$

where θ_1 and θ_2 are the polar angles of the two clusters. For a three particle final state with the third unobserved massless particle directed along the beam axis, x_z can be identified as the scaled energy of the unobserved particle, and for this case $x_z < 0.7$ corresponds to $m_{12}^2/s > 0.3$, where m_{12} is the mass of the two observed particles. These requirements define the kinematic acceptance used for measuring cross-sections in this analysis.

Secondly, in order to suppress backgrounds arising from cosmic-ray muon interactions or muons from the beam halo which can deposit significant energy in the calorimeter, we require that there is no activity in the detector consistent with a muon and that if either of

the two trigger clusters satisfies $|\cos\theta| < 0.75$ that the cluster extent is less than 250 mrad (see criteria B2 and B3 of [1] for details). We also require that these two clusters are separated by at least 30° in the transverse plane (i.e. $\phi_{\mathrm{acop}} < 150°$).

Thirdly, we designed criteria to reject events if they were consistent with a charged topology in that they contained at least one charged particle originating from the interaction point. We use two (three for $|\cos\theta| < 0.75$) detectors, namely, the silicon microvertex detector (for $|\cos\theta| < 0.75$), the vertex drift chamber axial wires and the jet chamber to form independent estimators of the existence of charged particle activity. Events where both trigger clusters have associated charged particle activity are rejected unless the only signal is from the jet chamber. Events where only one trigger cluster has associated charged particle activity are rejected if all (two or three) layers of charged particle detection registered activity. The veto efficiency was checked using Bhabha events and found to be $> 99.8\%$ for each layer per charged particle. Lastly, in order to address possible backgrounds from charged topologies such as $e^+e^- \rightarrow \ell^+\ell^-\gamma\gamma$, we required that there was no reconstructed track, with transverse momentum exceeding 1 GeV, separated from both trigger clusters by at least 15 degrees in azimuth. No events are rejected by this criterion.

A total of 103 events satisfy these selection criteria. Backgrounds from Bhabha scattering, $e^+e^- \rightarrow \tau^+\tau^-$, $e^+e^- \rightarrow$ hadrons, $e^+e^- \rightarrow \mu^+\mu^-$ have been considered and estimated to be negligible based on full detector simulation and the measured veto efficiency. All the events were visually examined to check for residual backgrounds. One event, interpreted as radiative Bhabha scattering in the (e)eγ topology where the observed positron undergoes hard bremsstrahlung in the vertex chamber end-plate, was identified as probable background and removed from the sample. The estimated efficiency for $e^+e^- \rightarrow \gamma\gamma(\gamma)$ is $(91.1 \pm 0.9)\%$ and for $e^+e^- \rightarrow \nu\bar{\nu}\gamma\gamma$ it is $(80 \pm 3)\%$. The inefficiency arises mainly from photons converting in the material located in front of the vertex chamber, and in the $\nu\bar{\nu}\gamma\gamma$ case also as a result of the opening angle requirement. The measured cross-sections are shown in Table 1. Their estimated systematic error is 2%.

The distributions of the scaled energy of the second and, possibly, third most energetic electromagnetic cluster are shown in Figs. 3(a) and (b) com-
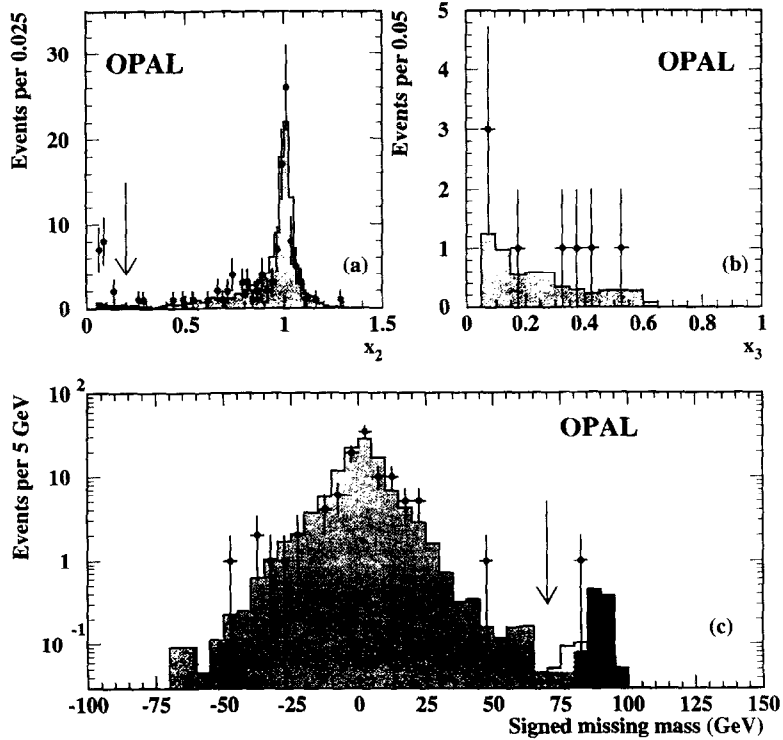
Fig. 3. Topology C. The data are represented by the points with error bars while the histograms show the predictions from Monte Carlo simulations for $e^+e^- \to \gamma\gamma(\gamma)$ (lightly shaded histogram), $e^+e^- \to \nu\bar{\nu}\gamma\gamma$ (dark histogram), and $e^+e^- \to \tau^+\tau^-$ (unshaded part of histogram). (a) Scaled energy of the second most energetic electromagnetic cluster (x_2). The cut at 0.2 is indicated by the arrow. It removes background not originating from e^+e^- collisions which is sizeable for x_2 below 0.1. The following distributions are shown for selected events. (b) The scaled energy (x_3) of a (possible) third most energetic electromagnetic cluster. Clusters with $x_3 > 0.05$ and $|\cos\theta| < 0.97$ were considered. (c) Measured signed missing mass of the two most energetic electromagnetic clusters. For cases where the measured missing mass squared is negative, the missing mass is evaluated as $-\sqrt{-m^2}$. The cut at 70 GeV, used to separate the $\nu\bar{\nu}\gamma\gamma$ contribution, is shown by the arrow.

pared to expectations from Standard Model processes. Good agreement is found. The number of selected events in which there is a third electromagnetic cluster with scaled energy exceeding 0.05 and $|\cos\theta| < 0.97$ is eight compared to 5.7 ± 0.4 such events expected. None of the selected events has a fourth electromagnetic cluster with scaled energy exceeding 0.05.

The expectation evaluated with full detector simulation includes the $\mathcal{O}(\alpha^3)$ QED expectation and the $\nu\bar{\nu}\gamma\gamma$ expectation evaluated using the event generator described in [15]. The expected cross-section for the latter process is calculated to be (0.23 ± 0.02) pb corresponding to 1.0 event expected.

A good separation between the two processes can be obtained in several variables, in particular the missing mass distribution shown in Fig. 3(c) motivates a cut

on the recoil mass against the two photons at 70 GeV. One of the selected events, recorded at $\sqrt{s} = 130$ GeV, has a measured recoil mass of $81.3 \pm 1.7 \pm 1.0$ GeV, and a large missing transverse momentum (18 GeV), which, given the detector hermeticity, is unexplainable by visible particles. The first error on the quoted recoil mass is from measurement error and the second is the estimated systematic error on the mass scale. The event properties are given in Table 2. This recoil mass is within four Breit-Wigner widths of the Z^0 peak and so may be explained by Z^0 mediated $\nu\bar{\nu}\gamma\gamma$ production.

The measured inclusive cross-sections and pure $\gamma\gamma(\gamma)$ cross-sections are presented in Table 1 and are compared to Standard Model expectations. Good agreement is found. The Born level cross-section can be obtained by applying a multiplicative factor
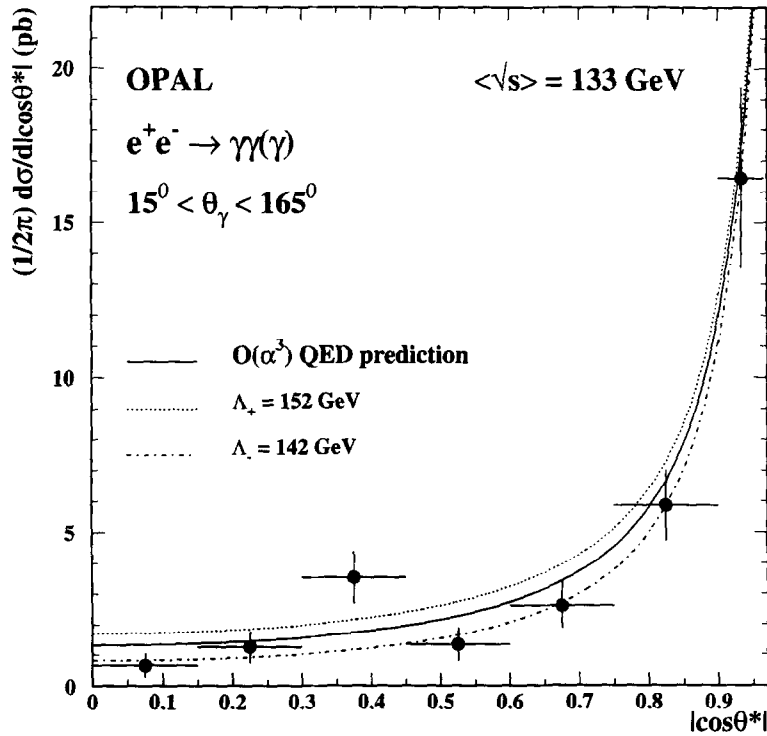
Fig. 4. The measured angular distribution for $e^+e^- \to \gamma\gamma(\gamma)$ events defining the event scattering angle using $|\cos\theta^*|$ as described in the text. The QED prediction at $\mathcal{O}(\alpha^3)$ (full line) is shown as calculated using the event generator of [16] with the kinematic acceptance stated in the text. The evaluated 95% CL lower limits on the cut-off parameters are indicated by dotted (Λ_+) and dash-dotted (Λ_-) lines.

of 0.950 to the measured cross-section for $e^+e^- \to \gamma\gamma(\gamma)$ displayed in Table 1.

The polar angle distribution for the 101 events selected with recoil mass below 70 GeV is shown in Fig. 4, and the measured differential cross-section is listed in Table 3. cosine of the event scattering angle has been defined using:

$$|\cos\theta^*| = \frac{|\sin(\theta_1 - \theta_2)|}{\sin\theta_1 + \sin\theta_2}.$$

This definition is identical to $|\cos\theta|$ in lowest order, and for three photon events with one photon collinear with the beams it is equivalent to the scattering angle in the centre-of-mass of the two observable photons. Correction factors for the detection efficiency in each angular bin have been evaluated using the fully simulated Monte Carlo events at $\mathcal{O}(\alpha^3)$. The angular distribution is compared to the $\mathcal{O}(\alpha^3)$ QED prediction where $|\cos\theta^*|$ for the prediction corresponds to the above definition for the two most energetic photons satisfying the kinematic acceptance. Note that the an-

Table 3
Measured differential cross-section for $e^+e^- \to \gamma\gamma(\gamma)$ defined as $\frac{1}{2\pi}\frac{d\sigma}{d|\cos\theta^*|}$ in pb. The $\frac{1}{2\pi}$ normalisation factor is to facilitate comparisons with data presented as $\frac{d\sigma}{d\Omega}$ in units of pb/sterad. The data have not been corrected back to the Born level.

$|\cos\theta^*|$ range	Events	$\frac{1}{2\pi}\frac{d\sigma}{d|\cos\theta^*|}$ (pb)
(0.0, 0.15)	3	0.7 ± 0.4
(0.15, 0.3)	6	1.3 ± 0.5
(0.3, 0.45)	17	3.5 ± 0.9
(0.45, 0.6)	6	1.3 ± 0.5
(0.6, 0.75)	12	2.6 ± 0.8
(0.75, 0.9)	26	5.9 ± 1.1
(0.9, cos 15°)	31	16.4 ± 3.0

gular distribution has *not* been corrected to the Born level. The data are consistent with QED, giving a χ^2 value of 15.9 for 7 degrees of freedom. Most of the χ^2 arises from the third bin in $|\cos\theta^*|$. Several models exist for possible deviations from QED. As a first example we show the sensitivity of the data to a possible

breakdown of QED, by introducing cutoff parameters $\Lambda_{\pm}$ following [21], such that the $|\cos\theta^*|$ distribution deviates from the $\mathcal{O}(\alpha^3)$ QED expectation as follows:

$$\frac{d\sigma}{d|\cos\theta^*|} = \frac{d\sigma}{d|\cos\theta^*|}\bigg|_{\text{QED}}$$
$$\times\left(1 \pm \frac{s^2}{2\Lambda_{\pm}^4}(1 - \cos^2\theta^*)\right).$$

We use a binned maximum likelihood fit to the number of events observed at each centre-of-mass energy in each angular bin following the method described in [3]. The normalisation is allowed to vary with an uncertainty of 2%. The fitted central value is $\Lambda^{-4} = (-0.7^{+1.1}_{-1.0}) \times 10^{-9}$ GeV^{-4}, consistent with zero. We determine 95% CL lower limits on Λ_+ and Λ_- of 152 GeV and 142 GeV, respectively, where for both models we have evaluated the limit by renormalising the probability to unit area within the physical region of the model ($\Lambda_{\pm} \geq 0$).

The differential cross-section for $e^+e^- \rightarrow \gamma\gamma$ would also be modified in a manner similar to the Λ_+ cut-off model by the presence of an excited electron [22]. In the $M_{e^*}^2 \gg s$ limit, the model parameters are related by $M_{e^*} = \sqrt{\lambda}\,\Lambda_+$, where M_{e^*} is the excited electron mass and λ is the coupling constant associated with the e*eγ vertex. We have fitted the differential cross-section using the same techniques as outlined above with the full formula for such a deviation given in [23]. For $\lambda = 1$, we set a 95% CL lower limit on the mass of an excited electron of 147 GeV based on a fitted central value for $M_{e^*}^{-4}$ of $(-0.7^{+1.2}_{-1.1}) \times 10^{-9}$ GeV^{-4}. Because of the fourth power dependence on centre-of-mass energy, the data presented here are as sensitive to these models as the most precise results published to date from e^+e^- collisions at the Z^0 [11].

6. Conclusions

Production of events with photonic final states has been measured in e^+e^- collisions at centre-of-mass energies of 130–140 GeV. The measured cross-sections shown in Table 1 are generally consistent with Standard Model expectations for the $e^+e^- \rightarrow \nu\bar{\nu}\gamma(\gamma)$ and $e^+e^- \rightarrow \gamma\gamma(\gamma)$ processes. The data on $e^+e^- \rightarrow \gamma(\gamma)$ + invisible particle(s) show

no evidence for anomalous single photon production. In total, six events with an acoplanar photon pair and large missing mass are found. The observed number of events is larger than expected from $e^+e^- \rightarrow \nu\bar{\nu}\gamma\gamma$; however, the missing mass distribution is compatible with the Z^0 resonance. Four of these events are selected by the search for events with an acoplanar photon pair topology, while 0.7 ± 0.1 events are expected from $\nu\bar{\nu}\gamma\gamma$. Deviations from QED are constrained by the data on $e^+e^- \rightarrow \gamma\gamma(\gamma)$. Lower limits are set at 95% CL on the QED cut-off parameters Λ_+ and Λ_- of 152 GeV and 142 GeV, respectively, and also on the mass of an excited electron of 147 GeV.

The L3 Collaboration has also reported measurements of photonic events at $\sqrt{s} \approx 133$ GeV in [24]. Their results on $e^+e^- \rightarrow \nu\bar{\nu}\gamma(\gamma)$ and $e^+e^- \rightarrow \gamma\gamma(\gamma)$ are consistent with Standard Model expectations and no evidence is found for excited neutrino pair production.

References

[1] OPAL Collab., R. Akers et al., Z. Phys. C 65 (1995) 47.

[2] OPAL Collab., P.D. Acton et al., Phys. Lett. B 311 (1993) 391.

[3] OPAL Collab., M.Z. Akrawy et al., Phys. Lett. B 241 (1990) 133.

[4] L3 Collab., B. Adeva et al., Phys. Lett. B 275 (1992) 209;
L3 Collab., O. Adriani et al., Phys. Lett. B 292 (1992) 463;
ALEPH Collab., D. Buskulic et al., Phys. Lett. B 313 (1993) 520;
DELPHI Collab., P. Abreu et al., CERN-PPE/96-03, submitted to Z. Phys. C.

[5] MAC Collab., W.T. Ford et al., Phys. Rev. D 33 (1986) 3472;
H. Wu, Ph.D Thesis, Univ. Hamburg, 1986;
CELLO Collab., H.-J. Behrend et al., Phys. Lett. B 215 (1988) 186;
ASP Collab., C. Hearty et al., Phys. Rev. D 39 (1989) 3207;
VENUS Collab., K. Abe et al., Phys. Lett. B 232 (1989) 431;
TOPAZ Collab., T. Abe et al., Phys. Lett. B 361 (1995) 199.

[6] A.D. Dolgov, L.B. Okun and V.I. Zakharov, Nucl. Phys. B 41 (1972) 197;
E. Ma and J. Okada, Phys. Rev. Lett. 41 (1978) 287;
K.J.F. Gaemers, R. Gastmans and F.M. Renard, Phys. Rev. D 19 (1979) 1605;
G. Barbiellini, B. Richter and J.L. Siegrist, Phys. Lett. B 106 (1981) 414.

[7] L3 Collab., M. Acciarri et al., Phys. Lett. B 346 (1995) 190; B 350 (1995) 109.

[8] H.E. Haber and D. Wyler, Nucl. Phys. B 323 (1989) 267;
S. Ambrosanio and B. Mele, Phys. Rev. D 53 (1996) 2541.

[9] C.H. Chen, M. Drees and J. Gunion, hep-ph-9512230, UCD preprint 95-43.

[10] OPAL Collab., M. Z. Akrawy et al., Phys. Lett. B 257 (1991) 531;
ALEPH Collab., D. Decamp et al., Phys. Rep. 216 (1992) 253;
DELPHI Collab., P. Abreu et al., Phys. Lett. B 327 (1994) 386.

[11] L3 Collab., M. Acciarri et al., Phys. Lett. B 353 (1995) 136.

[12] OPAL Collab., K. Ahmet et al., Nucl. Instrum. Methods A 305 (1991) 275;
P.P. Allport et al., Nucl. Instrum. Methods A 324 (1993) 34;
P.P. Allport et al., Nucl. Instrum. Methods A 346 (1994) 476;
B.E. Anderson et al., IEEE Transactions on Nuclear Science, 41 (1994) 845.

[13] LEP Energy Working Group, private communication.

[14] OPAL Collab., G. Alexander et al., Measurement of Cross-sections and Asymmetries in e^+e^- Collisions at 130–140 GeV Centre-of-mass Energy, CERN-PPE/96-025, submitted to Phys. Lett. B.

[15] F.A. Berends et al., Nucl. Phys. B 301 (1988) 583;
R. Miquel, C. Mana and M. Martinez, Z. Phys. C 48 (1990) 309.

[16] F.A. Berends and R. Kleiss, Nucl. Phys. B 186 (1981) 22.

[17] M. Böhm, A. Denner and W. Hollik, Nucl. Phys. B 304 (1988) 687;
F.A. Berends, R. Kleiss, W. Hollik, Nucl. Phys. B 304 (1988) 712;
D. Karlen, Nucl. Phys. B 289 (1987) 23.

[18] S. Jadach et al., Comp. Phys. Comm. 66 (1991) 276.

[19] J. Allison et al., Nucl. Instrum. Methods A 317 (1992) 47.

[20] G. Montagna et al., Nucl. Phys. B 452 (1995) 161.

[21] S.D. Drell, Ann. Phys. 4 (1958) 4.

[22] F.E. Low, Phys. Rev. Lett. 14 (1965) 238.

[23] A. Litke, Ph. D. Thesis, Harvard Univ., 1970.

[24] L3 Collab., M. Acciarri et al., Phys. Lett. B 370 (1996) 195, 211.